Tracing life through light: towards detecting life on exoplanets with spectroscopy and spectropolarimetry

Mulder, W.

Part II

Observing the Earth as an exoplanet using spectropolarimetry

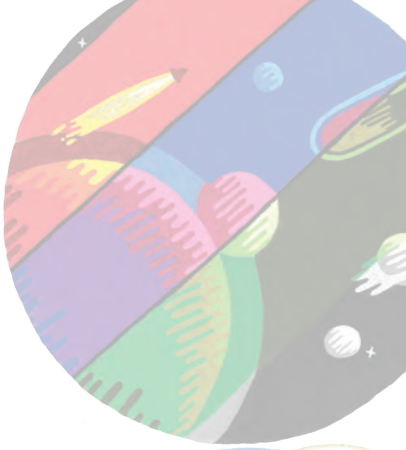

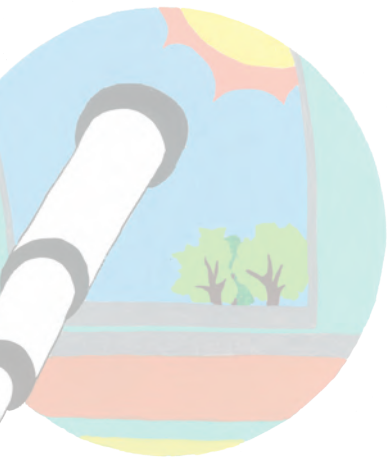

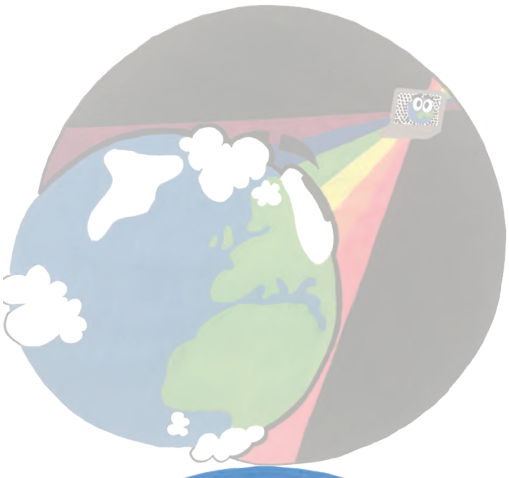

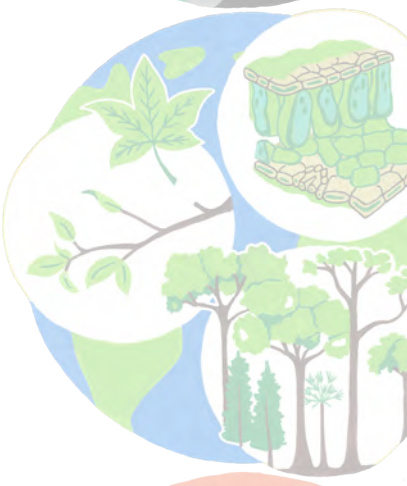


ANGRY
PHOTONS


THE
BEETLES

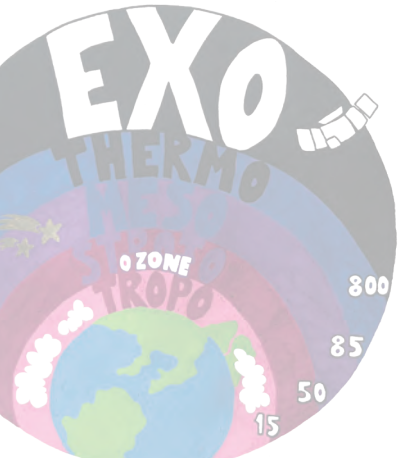
EXO
THERMO
OZONE
800
85
50
15

3 | Spectropolarimetric measurements of life from a hot-air balloon

Adapted from

Spectropolarimetry of life:
Airborne measurements from a hot-air balloon

W. Mulder, C. H. L. Patty, S. Spadaccia, A. Pommerol, B. O. Demory, C. U. Keller, J. G. Kühn, F. Snik, D. M. Stam

Light in Nature IX,
Proceedings of the SPIE, 12214, 1221404 (2022)

Does life exist outside our Solar System? A first step towards searching for life outside our Solar System is detecting life on Earth by using remote sensing applications. One powerful and unambiguous biosignature is the circular polarisation resulting from the homochirality of biotic molecules and systems. We aim to investigate the possibility of identifying and characterising life on Earth by using airborne spectropolarimetric observations from a hot-air balloon during our field campaign in Switzerland, May 30, 2022.

In this work we present the optical-setup and the data obtained from aerial circular spectropolarimetric measurements of farmland, forests, lakes and urban sites. We make use of the well-calibrated FlyPol instrument that measures the fractional circular polarisation (V/I) of light with a sensitivity of $< 10^{-4}$. The instrument operates in the visible spectrum, ranging from 400 to 900 nm. We demonstrate the possibility to distinguish biotic from abiotic features using circular polarisation spectra and additional broadband linear polarisation information. We review the performance of our optical-setup and discuss potential improvements. This sets the requirements on how to perform future airborne spectropolarimetric measurements of the Earth's surface features from several elevations.

3.1 Introduction

The remote-sensing of the Earth gives us indispensable information for our preparations to search for extraterrestrial life. Well-known examples of biosignatures that can be identified in the reflected sunlight are atmospheric constituents such as O_2 and spectral signatures of vegetation, such as the green bump and the red edge (see Seager et al., 2005, for a detailed description of the red edge). In addition, spectropolarimetry proves itself to be a robust remote-sensing tool. Complementary to the reflectance, it carries additional and unique information, such as surface roughness or particle size of the scatterers, which helps us to look for and characterise bio-signatures. Spectropolarimetry also provides unique biosignatures itself, such as the linear polarisation resulting from the O2-A band (Stam et al., 1999; Fauchez et al., 2017) and from vegetation (Vanderbilt et al., 1985, 1991), as well as circular polarisation resulting from the homochirality of biotic systems (Patty et al., 2019; Gimenez et al., 2019).

Homochirality is what we refer to as the single handedness of chiral molecules. Terrestrial chiral molecules that are utilised by life, e.g. amino acids, sugars and the biological polymers they construct, almost always exists in either left-handed or right-handed forms, and are therefore homochiral. This is in contrast to abiotic chemistry, which produces equal amounts of these mirror forms, resulting in a racemic mixture. Circular polarisation originates from the differential absorption by homochiral molecules and macromolecular structures. As biochemical homochirality is essential for life and thought to be a universal property of life, the circular polarisation life produces constitutes an unambiguous bio-signature (Patty et al., 2018a). Therefore, circular polarisation promises to be a powerful tool for the remote-sensing of biotic matter on Earth (Wolstencroft et al., 2004; Patty et al., 2017, 2019; Patty et al., 2021) and beyond (Sparks et al., 2005; Patty et al., 2018a).

In general, direct light emitted by a solar type star is virtually unpolarised when integrated across its stellar disk (Kemp et al., 1987). Since linear polarisation is produced by interaction of light with surfaces and particles, whenever Sunlight interacts with the Earth's atmosphere or surface, it usually becomes (partly) linearly polarised. As such, we do find an abundance of polarised light by looking at the Earth's atmosphere or surface. Various of these polarising scattering mechanisms, like Rayleigh scattering and reflections at air-water interfaces, are well understood (Cronin & Marshall, 2011). Despite all this knowledge, the interpretation of remotely sensed linear polarisation data of the real world is challenging as it involves e.g. depolarisation effects, varying atmospheric aerosol concentrations and a diversity of (cloud)particle phases, shapes, and orientations.

Circularly polarised light is much more scarce in nature. It can be produced through multiple scattering processes. Single scattering processed usually generate linearly polarised light, after which a second scattering event with atmospheric aerosols can produce circularly polarised light. We refer to Gassó & Knobelspiesse (2022) for an elaborate summary of circular polarisation due to atmospheric aerosols. In addition to multiple scattering processes, circularly polarised light can be produced by the homochirality of biotic systems (Patty et al., 2019; Patty et al., 2021).

The development of theoretical scattering models including both linear and circular polarisation is essential to understand all information coming from remotely sensed spec-

tropolarimetric data. There exist various extensive spectropolarimetric models of Earth-like (exo)planets featuring realistic atmosphere profiles (Stam, 2008) realistic cloud parameters (Groot et al., 2020), wind-ruffled oceans with sea foam and shadows of the waves (Trees & Stam, 2022) and multiple surface reflection scattering matrices based on bidirectional reflectance functions and characteristic (wavelength-dependent) surface albedos (Stam, 2008). For the latter, surface albedos for many different natural and man-made materials are provided by libraries such as the ASTER (Baldridge et al., 2009) and the ECOSTRESS spectral library (Meerdink et al., 2019).

Surface albedos can be used for surface identification. For example, the spectral shapes of vegetation features can be easily distinguished from bare soils (Liang et al., 2002), see Fig. 3.1. Albedos might vary over the year due to the change of seasons, change in vegetation characteristics or their moistness. The vegetation albedo spectra share the following characteristics: (i) absorption bands of chlorophyll around 435 – 485 nm and around 645-685 nm, (ii) a high albedo at wavelengths longer than 700 nm, which is also referred to as the red edge and (iii) the absorption of light due to intracellular liquid water causing slight dips around 0.97, 1.15, 1.45, and 1.92 μm (Hegde et al., 2015). The definition of surface albedo is commonly used in the field of astronomy and climate research. For simplicity, we will refer to the surface albedo as the (surface) reflectance.

Even though there has been an extensive advancement of the models over the years, there is still room for improvement. The surface models derived from scattering matrices based on the surface reflectance serve their purpose very well when considering a planetary disk-integrated signal. Unfortunately, they do not include circular polarisation signals induced by vegetation features. In general, and especially in nature, circular polarisation signals are very faint compared to those of linear polarisation: the difference can easily be three orders of magnitude. However, being a powerful tool for the remote-sensing of biotic matter, we do want to investigate the possibility of adding circular polarisation to existing surface models.

Remote-sensing of (circularly) polarised biosignatures has received a lot of interest in recent years (Patty et al., 2019; Patty et al., 2021; Snik et al., 2019; Sparks et al., 2020). Data acquired through remote-sensing offers crucial information for preparation for the design and development of the next generation of space-based spectropolarimeters. We follow up upon the results of Patty et al. (2021). They used a helicopter to perform airborne measurements. In this work, we are using a stable and cheaper airborne platform: a hot-air balloon. One of the biggest advantages of a hot-air balloon is that our proximity to our instrument during the flight allows us make on the fly adjustments to the optical-setup. We measure the light that is reflected by the surface from the moving balloon basket. Hence, a single measurement is limited to a single illumination angle, viewing angle and elevation. Therefore, our main focus lies with measuring the circular polarisation spectra from landscapes and their use in surface identification. In addition to circular polarisation, we continuously record four individual linear polarisation states using an ordinary polarisation camera. We investigate the contribution and practicality of using a polarisation camera for future airborne field campaigns.

This chapter has the following structure. In Section 3.2, we describe the basics of polarimetry and the concept of the normalised difference vegetation index to distinguish between different surface types. In Section 3.3, we describe our instrumental set-up that was designed to measure the fractional circular polarised reflection of the Earth from a balloon.

In Section 3.4, we summarise the main results from the airborne measurements. At the end, we finalise this chapter with our conclusions and discussion in Section 3.5.

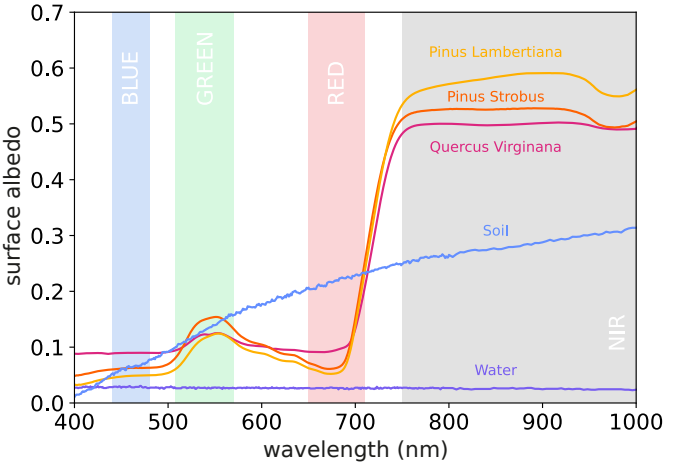

Figure 3.1: The wavelength dependent surface albedos of 3 different types of trees, (i) Quercus Virginana, (ii) Pinus Strobus, and (iii) Pinus Lambertiana, and soil and water. The data for the five albedos originate from the ECOSTRESS Spectral Library (Meerdink et al., 2019).

3.2 Methods

3.2.1 Polarisation

Polarisation is generally described with a Stokes vector $\mathbf{S} = (\mathtt{I}, \mathtt{Q}, \mathtt{U}, \mathtt{V})$, where $\mathtt{I}$ is the total intensity, $\mathtt{Q}$ and $\mathtt{U}$ are the linearly polarised intensities and $\mathtt{V}$ the circularly polarised intensity. The complete polarisation states are described in terms of the normalised Stokes parameters $\mathtt{Q/I}$, $\mathtt{U/I}$ and $\mathtt{V/I}$ (each ranging from -1 to 1), where $\mathtt{Q/I}$ denotes the difference between linearly polarised intensities normal and parallel to the plane of scattering, $\mathtt{U/I}$ denotes the difference between ±45° to the plane of scattering, and $\mathtt{V/I}$ denotes the difference between right-handed and left-handed circularly polarised light.

The linear Stokes parameters $\mathtt{Q}$ and $\mathtt{U}$ can be combined into the (dimensionless) degree of linear polarisation, P_L. The P_L of a surface indicates the fraction of the reflected light that is linearly polarised. It can provide us with essential information about land surface characteristics. The angle of linear polarisation, χ_L, contains additional information related to surface or material properties. The degree and angle are expressed as:

$$P_\mathrm{L} = \frac{\sqrt{\mathtt{Q}^2 + \mathtt{U}^2}}{\mathtt{I}}; \quad \chi_\mathrm{L} = \frac{1}{2}\tan^{-1}\left(\frac{\mathtt{U}}{\mathtt{Q}}\right). \tag{3.1}$$

3.2.2 The normalised difference vegetation index

Using satellite imaging techniques, we can measure the reflected light spectra of different types of terrestrial surfaces. However, calculating an accurate widespread surface reflectance can be complex. Instead, we choose to calculate the normalised difference vegetation index (NDVI; Rouse et al., 1974) for individual measurements to distinguish between different surface types. We calculate the NDVI similar to Patty et al. (2021)

$$\mathrm{NDVI} = \frac{I_{\mathrm{NIR}} - I_{\mathrm{R}}}{I_{\mathrm{NIR}} + I_{\mathrm{R}}}, \tag{3.2}$$

where I_{R} is the mean of the reflectance from 650 – 710 nm and I_{NIR} from 750 – 780 nm.

By definition, the NDVI ranges from –1.0 to +1.0. Negative values generally correspond to water. Values approaching +1.0 typically indicate dense green vegetation: plants absorb most solar radiation between 400 and 700 nm for photosynthesis, while strongly reflecting light in the near-infrared (the 'red edge'). As a result, for healthy vegetation I_{NIR} is much larger than I_{R}, giving NDVI values close to 1.0. Values around zero indicate little or no green vegetation, such as urban surfaces like roofs, roads, and/or concrete.

3.3 Instrumental set-up

The circular spectropolarimetric measurements presented in this work were performed using the FlyPol instrument (Patty et al., 2021). FlyPol is a spectropolarimeter based on the TreePol design (Patty et al., 2017, 2019). It uses fast temporal polarisation modulation to measure the fractionally induced circular polarisation (V/I) as a function of wavelength, from 400 to 900 nm. Its sensitivity ($< 10^{-4}$) and accuracy ($< 10^{-3}$) are sufficient to measure less than a tenth of a percent of the incident light that may become circularly polarised after reflection from biological samples, e.g. vegetation. To improve stability during fieldwork, FlyPol actively controls the temperature of its optics and electronics. Its angular field of view is approximately 1.2° (Patty et al., 2021).

All airborne measurements presented in this chapter were collected during a single flight in an Ultramagic hot-air balloon (8,500 m^3) equipped with a T-partition basket with a capacity of 11 passengers including the pilot. Four scientists were allowed to join the campaign, because of the relatively large basket ($3.05 \times 1.75 \times 1.20$ m) A single partition was sufficiently large enough ($\sim 2.00 \times 0.80$ m) to unfold ans secure the tripod on which FlyPol was mounted. All electronics were stored beneath the tripod, leaving enough space to manually point the instrument and perform potential small repairs.

FlyPol was oriented using a calibrated parallax-free telescope pointer (Patty et al., 2021). A GoPro HERO7 reference camera and a broadband Thorlabs polarisation-sensitive Kiralux® camera were aligned with the pointer and mounted on top of the instrument casing, see Fig. 3.2. The polarisation camera features a monochrome CMOS detector with a wire-grid polariser array consisting of a repeating pattern of four linear polarisers oriented at 0°, 45°, 90°, and 135°. One combination of these four pixels with these orientations is referred to as a super-pixel. A super-pixel calibration algorithm (Gimenez et al., 2019; Lane et al., 2022)

corrects the images for dark noise, flat-field variations, and optical imperfections in the polarisation filter array. This setup provides pointing information and additional context for the observed areas, which is useful during data analysis.

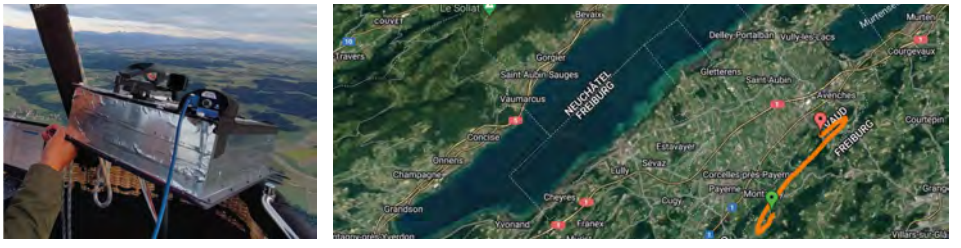

Figure 3.2: **Left panel:** Photo of the instrument set-up on top of a tripod pointing over the edge of the hot-air balloon basket, during the flight. **Right panel:** Map of the flight trajectory.

Two individual GPS trackers were used to record the flight trajectory, see Fig. 3.2. The balloon flew over the Broye district in the canton of Fribourg, Switzerland. This region lies on an elevated, relatively flat plain that is called the Swiss Plateau. The canton is predominantly rural, featuring farm sites, valleys and small forests. With an altitude of 2389 m, the Vanil Noir is the highest mountain in the canton. This is about 200 m lower than the highest altitude that we reached during our flight. Hereon we refer to the elevation of the balloon, which is the difference between measured GPS altitude in the air and the local ground-level altitude. The highest elevation was just below 2000 m. The wind determines both the flight speed and direction. At altitudes < 1500 m we were heading south with a ground speed of ~ 10 km/h, while the winds at altitudes > 1500 m droves us north with a ground speed of $\sim$27 km/h. The pilot could turn the orientation of the balloon, and thus the basket, in the time frame between the end of the take-off and the start of the landing.

In total, 31 measurements were obtained under clear sky conditions on May 30, 2022, from 19:45 to 20:45 CEST, just before sunset (21:20 CEST). We choose to fly during the evening hours, as hot-air balloons are only able to fly within the time-span of three hours before sunset until three hours after sunrise. In this work, we refer to a single, continuous measurement as a *scene*. During the flight, the solar zenith and azimuth angle were approximately $86° - 90°$ and $300° - 310°$, respectively. Throughout the flight, FlyPol's integration times were varied per *scene* to obtain the highest average photon count possible while preventing saturation, see Fig. 3.3. For the first and last measurements, the average photon count (< 10000 counts) is low compared to the later measurements. While approaching sunset, the integration time increased as the photon counts strongly decreased with time. At the same time, we adjusted the integration times of the polarisation camera, as the auto-exposure mode caused saturation of the first set of images. The polarisation camera was set to record one exposure every five seconds. Unfortunately, adjusting the integration times took at least a minute, leaving holes in the dataset. The reference camera took automatic shutter images every 30 seconds[1].

[1] 30 seconds is the minimum interval for automatic shutter imaging with the GoPro HERO7.

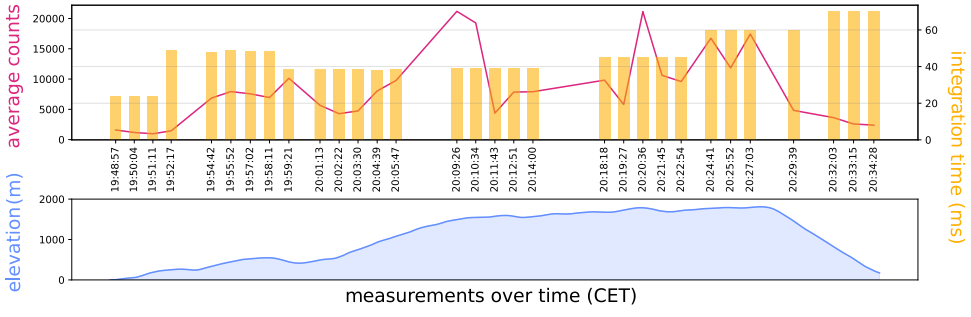

Figure 3.3: **Top panel:** The average spectrometer raw photon count over a given integration time for the individual *scenes*. **Bottom panel:** The elevation of the balloon during the flight (hence distance to the ground).

3.4 Results

In Fig. 3.4, we show the results of a *scene* observed during take-off, at an elevation of about 20 m. The reference photo on the left contains three transparent black/white dots that mark the central pointing of FlyPol for three sequential measurements with a 30 seconds time interval. The line connecting the dots indicates the likely intermediate pointing trajectory. The panels on the right show the qualitative reflectance and circular polarisation V/I for the trajectory per wavelength, over time. Both plots show a very clear separation between the reflected light signals of the soil and the grass after ~ 400 measurements. The soil shows a spectrally flat reflectance and a negligible circular polarisation. The grass shows a strong increase in the reflectance in the red edge, around 710 nm. The inset in the left image reveals the circular polarisation spectrum averaged over time for the soil and grass features on the right. The grass spectrum reveals a negative band with a minimum at 675 nm with a magnitude of $\mathrm{V/I}_{\mathrm{min}} = 2.0 \cdot 10^{-3}$.

In Fig. 3.5 we show the results for a *scene*, pointing at a rural area from an elevation of ~ 650 m. The yellow and pink lines in the white line trajectory match the location of the in yellow and pink highlighted qualitative reflectance data for the trajectory per wavelength, over time. We were able to identify the two different surface types using the reflectance and the NDVI. Just as for the reflectance in Fig. 3.4, there is an increase in the reflectance around 675 nm due to the red edge. The measured V/I is smaller than for the previous *scene*.

Using the NDVI values and the reference photos for the individual *scenes*, we were able to differentiate between five surface types; grass, soil, trees, urban, and water. The spectra presented in Fig. 3.6 are time averaged V/I spectra. The *scenes* that feature vegetation (grass, trees) are easily distinguishable from the others, due to their high (> 0.75) NDVI values. As explained earlier, this is due to the relative strong reflection of near-infrared light and absorption of red light by the chlorophyll molecules. The circular polarisation spectra of trees had a positive polarisation band of $\mathrm{V/I} = 1.0 \cdot 10^{-3}$ around 650 nm. The grass has a

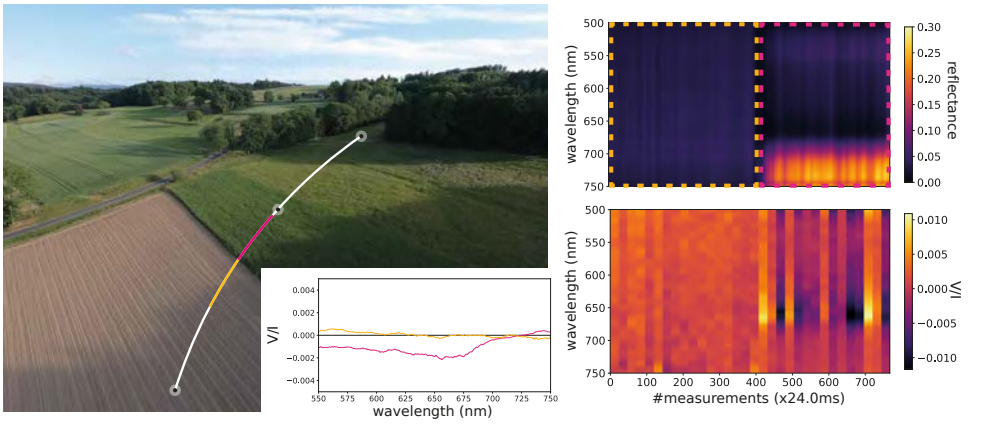

Figure 3.4: **Right panel:** Single measurement *scene* during take-off near Montagny, at 19:48:57 CEST at an elevation of ~ 20 m and with a ground speed of ~ 5 km/h. The transparent black/white dots mark the pointing of FlyPol for three sequential measurements with a 30 seconds time interval. The inset indicates the circular polarisation spectrum averaged over the individual soil and grass *scenes* in yellow and pink, respectively. **Top right panel:** Qualitative reflectance spectra for the full trajectory. **Bottom right panel:** `V/I` spectra for the full trajectory.

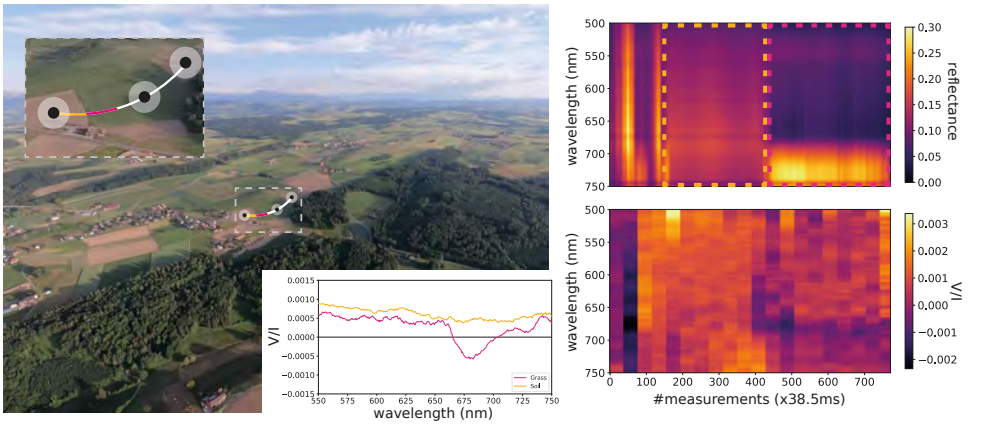

Figure 3.5: Similar to Fig. 3.4, except at 20:01:13 CEST, with an elevation of ~ 650 m and a ground speed of ~8.5 km/h.

negative band with a minimum of $\mathtt{V/I} = 2.0 \cdot 10^{-3}$ around 660 nm. Beyond ~ 675 nm, `V/I` decreases. As expected, *scenes* that feature the soil, urban and water do not show significant circular polarisation signals.

Patty et al. (2021) flew over the lake Lac des Taillères and measured a circular polarisation

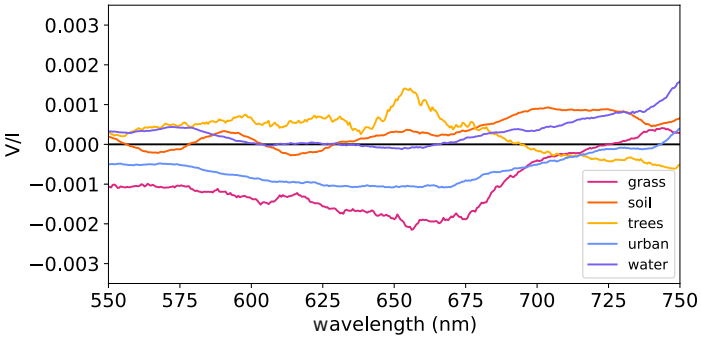

Figure 3.6: V/I spectra measured while pointing at various surfaces *scenes*: grass, soil, trees, urban, and (lake) water.

signal of $V/I = 1.1 \cdot 10^{-3}$, which indicates a possible presence of photosynthetic organisms like algae. Multiple measurements were taken while pointing towards the Murtzensee, resulting in the time-averaged V/I spectra of Fig. 3.7. From these spectra, we concluded that there was no detection of circular polarisation while pointing at the lake, which suggests an absence of biotic organisms.

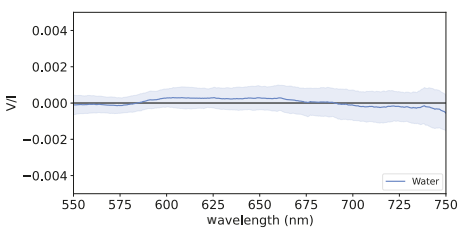

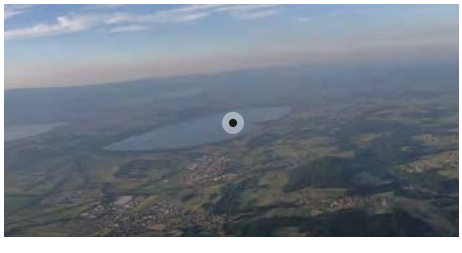

Figure 3.7: **Left panel:** Flat V/I spectra measured while pointing towards the Murtzensee. **Right panel:** Reference photo of the observed *scene* during take-off (20:12:51 CEST with ~1870 m elevation and ~25.0 km/h ground speed) flying in a NE direction.

Figures 3.8 and 3.9 illustrate the difficulty of identifying multiple distinct surface features within one *scene*. Figure 3.8 contains 15 subsequent three-second duration circular polarisation spectra originating from one observation *scene* while flying over farmland. The magnitude varies from $V/I_{min} = -9.0 \cdot 10^{-3}$ to $V/I_{max} = 2.5 \cdot 10^{-3}$ due to a large variety of observed grass and soil. This large variety makes it difficult to designate an accurate source to all the individual lines. We end up with a signal of $V/I = 2.0 \cdot 10^{-3}$, see pink line in Fig. 3.8, when averaging over all 15 spectra. The three spectra, large-, no- and small red edge, presented in Fig. 3.8 are also originating from one observation *scene*. The 'small red edge'-spectra shows one positive band of $V/I = 1.0 \cdot 10^{-3}$, where the 'large red edge'-spectra shows a similar positive band and a large negative band of $V/I = -4.2 \cdot 10^{-3}$. By looking at the trajectory, we identify the small and the large red edge as grass and trees respectively. The

circular polarisation spectrum averaged over the entire *scene* does not reveal a clear circular polarisation signature due to the relative large soil ('no red edge') coverage across the *scene*.

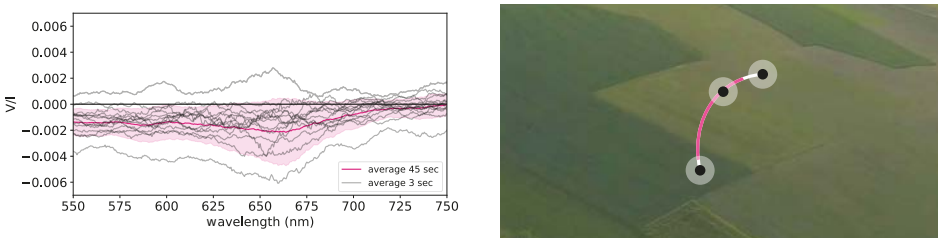

Figure 3.8: **Left panel:** 15 subsequent three-second-averaged and the total 45-second-averaged circular polarisation spectra. The *scene* captures farmland that features various types of grass and soil. **Right panel:** Reference photo of a *scene* during take-off (19:52:17 CEST at ~ 790 m elevation and ~ 7.8 km/h ground speed) flying towards Ruisseau de Pra Laurent, in the S direction while pointing at farmland. The colours on the white trajectory indicate the measurement locations of the `V/I` spectra displayed in the left figure.

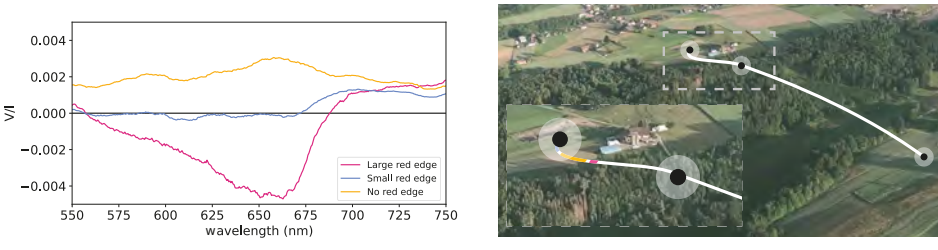

Figure 3.9: **Left panel:** Time-averaged `V/I` of a large, a small and no red edge effect, identified as trees, grass and soil respectively. **Right panel:** Reference photo of a measurement *scene* during take-off (19:54:42 p.m. CEST with ~540 m elevation and ~ 3.9 km/h ground speed) flying towards Mannens-Grandsivaz, flown in SW direction while pointing towards Marais Martin.

From top to bottom, Fig. 3.10 shows four polarisation camera images of the Murtensee and its coast, a distant mountain top, a central point of the Murtensee and an urban landscape. The images capturing the degree of linear polarisation reveal structural features of the landscapes. This allows us to e.g. distinguish a mountain top covered in ice from foggy clouds that are located just above the horizon. For the urban landscape (the middle bottom plot), we clearly distinguish the (white) buildings located in the lower half of the image from the grass fields located in the top half of the image. The angle of linear polarisation of the 'Murtzensee' and 'Glint Murtzensee' images reveal a patchy structure on the water surface that we identify as a glint phenomenon.

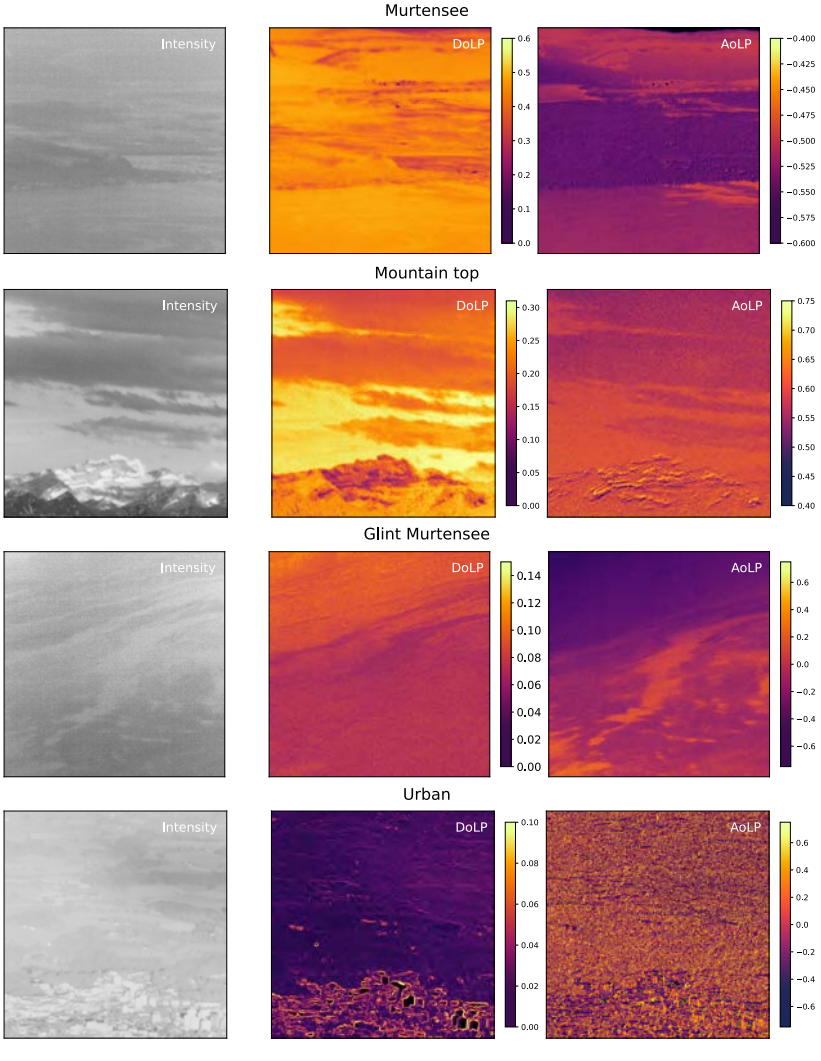

Figure 3.10: 600 × 600 pixel cut-out of polarisation camera images. **Panels top to bottom**: Murtensee and its coast, distant mountain top, the Murtensee featuring a glint and urban landscape. **Panels left to right**: Intensity, degree- and angle of linear polarisation maps, see Eq. 3.1. Note that the detector edges reveal polarisation artifacts with strong gradients, producing false signals within the super pixels on the polarisation camera.

3.5 Conclusion & discussion

We described an airborne optical-setup that we used to simultaneously measure circular polarisation spectra and broadband degree- and angle of linear polarisation from various *scenes* that include biotic and abiotic features. During the entire flight, reference photos were taken with a regular imaging camera. These encapsulated the area that we were pointing towards, allowing for concise identification of the sources inducing the observed the circular polarisation spectra. To our knowledge, this was the first time that a hot-air balloon was used as an observing platform for spectropolarimetric measurements of the Earth's surface. We established the maximum solar angle and integration time for which we can obtain circular polarisation spectra. This information is of great value for the next upcoming flights.

At elevations of ~ 20 m and ~ 650 m, we could distinguish between circular polarisation spectra of grass and soil. The spectral characteristics of the grass landscapes in this chapter are qualitatively similar to those presented by Patty et al. (2021). We measured a circular polarisation of grass of $\mathtt{V/I} = 2 \cdot 10^{-3}$ (~ 20 m elevation) and $\mathtt{V/I} = -5 \cdot 10^{-4}$ (~ 650 m elevation). Unlike Patty et al. (2021), we did not observe any presence of circular polarisation in sunlight reflected by lake water. A possible explanation is that there is a smaller biomass of photosynthetic organisms in the water, as this study was conducted in the early spring, while patty et al. measured during late summer. In addition, the lake was observed in the second half of the balloon flight, close to sunset. The lack of signal could thus also be due to the combination of a large viewing and solar angle.

We were able to capture how V/I varies for a subsequent observation of farmland featuring various types of grass and possibly dry, and wet soil types. The circular polarisation spectra for 15 subsequent three-second duration measurements of the farm land reveal the circular polarisation ranging between $\mathtt{V/I} = -9.0 \cdot 10^{-2}$ and $\mathtt{V/I} = 0.25 \cdot 10^{-2}$. We have two explanations for this variation: (i) the arrangement of e.g. crops in soil causes the variation as we interchange observing crops and soil, or (ii) the variation is a consequence of a diversity in health of the observed vegetation. The latter explanation is the more likely one, as we do not see clear crop(-like) fields on the reference photo. Although quantitative circular polarisation measurements on the health of the vegetation are lacking, we do know that leaves so show a reduced circular polarisation when decaying (Patty et al., 2017). Further quantitative and qualitative analysis is required to verify our hypothesis.

The circular polarisation spectra from grass feature solely a single band, often being negative. Unlike the grass spectra, those from tree canopies show vary both from shape and sign. The forest spectra, as presented in Patty et al. (2021), have both a positive and negative band that exhibit a larger variation in shape and magnitude than the grass spectra. The difference between the two is illustrated in Fig. 3.9. The spectra showing the large negative peak is identified as grass, whereas the single positive peak around 710 nm appears to be induced by tree canopies. During this field campaign, we noticed a high diversity in circular polarisation spectra for forests. It remains unclear what mechanisms could cause these variations. Measurements performed on individual (tree) leaves is a first step towards understanding the signals resulting from a canopy. As far as we know, Patty et al. (2022) is the only study that

investigated the full-Stokes spectropolarimetry of single leaves from different species and its dependency on the incidence angle of the light source. In their experiment, they varied between a phase angle of $10° - 75°$ where the phase angle is similar to the angle of the incident light. In general, all their fractional linear (`Q/I`) polarisation spectra show a peak around 680 nm due to absorption by chlorophyll and all their fractional circular (`V/I`) spectra feature a negative band around 670 nm and a positive band around 700 nm. The `Q/I` spectra reveal a strong dependence on phase angle, whereas the `V/I` spectra are relatively insensitive to changes in the phase angle. We are currently investigating the effect of changing the phase angle and viewing angle of multiple-, leaf-to-leaf reflections. With this knowledge, we will be a step closer to formulate a realistic circular polarisation surface model that can be used to accurately simulate various tree canopies and therefore also aid in the interpretation of airborne full-Stokes spectropolarimetric measurements. In addition, these realistic circular polarisation surface models would be valuable for realistic Earth-like (exo)planet models (Stam, 2008; Groot et al., 2020).

We used the obtained broadband degree- and angle of linear polarisation information for landscape identification purposes. It would be interesting to capture linear polarisation spectra together with our circular polarisation spectra of the surface *scenes*. This can be achieved by either adding a second spectropolarimeter or a spectropolarimeter that is capable of acquiring full-Stokes polarisation from a single data frame (Snik et al., 2019; Sparks et al., 2019; Keller et al., 2020; Mulder et al., 2021). Peltoniemi et al. (2015) points out that linear polarisation would predominantly provide scalar reflectance information. However, we might be able to obtain more information than surface reflectance, especially when covering multiple phase angles.

Due to the relatively fast ascend and descend, the effect of the balloon elevation on the circular polarised spectra from abiotic and biotic surfaces remains inconclusive. Further research (including numerical simulations) will help us to understand the influence of illumination, viewing angles on the circular polarisation spectra for various landscapes including high elevation biomes (e.g. tundra, moss, lichens), barren land, possible water bodies (in shallow water) ice, snow, and red algae on snow from different elevations. Hot-air balloons are only able to fly within the timespan of three hours before sunset until three hours after sunrise. We will plan our next balloon flight in the early morning. This allows us to prepare our instrument during take-off, e.g. taking flat fields, while setting up the polarisation and reference camera. Doing so, we are able to start the observations just after sunrise, which prevents long integration times and large scattering angles. In upcoming research, we would like to include measurements of grass and various tree canopies from one single observation point over the course of a full day. With this quantitative and qualitative data, we will be able to formulate a realistic circular polarisation vegetation model.

3.6 Acknowledgements

We thank the team of Balloons du Leman (the entire ground team, Julie, pilot Laura and Gael) personally for their enthusiasm, flexibility and help in the preparations for and during the balloon flight. We thank Remko Stuik for the airborne platform brainstorm session. This work has been carried out within the framework of the NCCR PlanetS supported by the Swiss National Science Foundation under grants 51NF40_182901 and 51NF40_205606. This work was supported by the second Planetary and Exoplanetary Science Programme (PEPSci-II) of the Netherlands Organisation for Scientific Research (NWO).